ANTIOXIDANTS & REDOX SIGNALING
Volume 24, Number 11, 2016

DOI: 10.1089/ars.2015.6442

Therapeutics

ORIGINAL RESEARCH COMMUNICATION

Methionine Sulfoxide Reductase B3-Targeted *In Utero* Gene Therapy Rescues Hearing Function in a Mouse Model of Congenital Sensorineural Hearing Loss

Min-A Kim,[1,2] Hyun-Ju Cho,[1] Seung-Hyun Bae,[1,2] Byeonghyeon Lee,[1,2] Se-Kyung Oh,[1–3] Tae-Jun Kwon,[4] Zae-Young Ryoo,[5] Hwa-Young Kim,[6] Jin-Ho Cho,[7] Un-Kyung Kim,[1,2] and Kyu-Yup Lee[8]

Abstract

Aims: Methionine sulfoxide reductase B3 (MsrB3), which stereospecifically repairs methionine-*R*-sulfoxide, is an important Msr protein that is associated with auditory function in mammals. *MsrB3* deficiency leads to profound congenital hearing loss due to the degeneration of stereociliary bundles and the apoptotic death of cochlear hair cells. In this study, we investigated a fundamental treatment strategy in an *MsrB3* deficiency mouse model and confirmed the biological significance of *MsrB3* in the inner ear using *MsrB3* knockout (*MsrB3*$^{-/-}$) mice. ***Results:*** We delivered a recombinant adeno-associated virus encoding the *MsrB3* gene directly into the otocyst at embryonic day 12.5 using a transuterine approach. We observed hearing recovery in the treated ears of *MsrB3*$^{-/-}$ mice at postnatal day 28, and we confirmed *MsrB3* mRNA and protein expression in cochlear extracts. Additionally, we demonstrated that the morphology of the stereociliary bundles in the rescued ears of *MsrB3*$^{-/-}$ mice was similar to those in *MsrB3*$^{+/+}$ mice. ***Innovation:*** To our knowledge, this is the first study to demonstrate functional and morphological rescue of the hair cells of the inner ear in the *MsrB3* deficiency mouse model of congenital genetic sensorineural hearing loss using an *in utero*, virus-mediated gene therapy approach. ***Conclusion:*** Our results provide insight into the role of MsrB3 in hearing function and bring us one step closer to hearing restoration as a fundamental therapy. *Antioxid. Redox Signal.* 24, 590–602.

Introduction

MOLECULAR OXYGEN, WHICH is used for numerous processes during aerobic metabolism in cells, is related to the generation of reactive oxygen species (ROS) (18). ROS, such as superoxide anion, hydrogen peroxide, and hydroxyl radical, can oxidize cell components, including nucleic acids, intracellular proteins, and lipids, and induce cell death (22, 45, 47). Both the polypeptide backbone and amino acid residue side chains of proteins can also be targeted (5, 47, 48), and sulfur-containing amino acids such as methionine (Met) and cysteine (Cys) are the most susceptible to oxidation by ROS (5). However, some of these modifications can be repaired by defense systems that protect against oxidative stress (23, 33, 34, 41, 44, 46). Met residues are converted to Met-*S*-sulfoxide and Met-*R*-sulfoxide by oxidative stress and are repaired by stereospecific enzymes such as Met sulfoxide reductase A (MsrA) and B (MsrB1, MsrB2, and MsrB3) (23, 26, 46, 49, 50, 53). In addition, the Met/Msr system may aid other redox systems to maintain cellular redox homeostasis (26).

Due to the physiological importance of the Met/Msr system in mammals, several studies in animal models have

[1]Department of Biology, College of Natural Sciences, Kyungpook National University, Daegu, Republic of Korea.
[2]School of Life Sciences, KNU Creative BioResearch Group (BK21 plus project), Kyungpook National University, Daegu, Republic of Korea.
[3]Division of Life Sciences, Korea Polar Research Institute (KOPRI), Incheon, Republic of Korea.
[4]Laboratory Animal Center, Daegu-Gyeongbuk Medical Innovation Foundation (DGMIF), Daegu, Republic of Korea.
[5]School of Life Science and Biotechnology, College of Natural Sciences, Kyungpook National University, Daegu, Republic of Korea.
[6]Department of Biochemistry and Molecular Biology, Yeungnam University College of Medicine, Daegu, Republic of Korea.
[7]Department of Electronic Engineering, College of IT Engineering, Kyungpook National University, Daegu, Republic of Korea.
[8]Department of Otorhinolaryngology-Head and Neck Surgery, School of Medicine, Kyungpook National University, Daegu, Republic of Korea.

Innovation

Methionine sulfoxide reductase B3 (MsrB3) is important for the maintenance of hair cells, and the mutations in the *MsrB3* gene are associated with human autosomal recessive nonsyndromic hearing loss. The present work provides the first demonstration of functional and morphological rescue of the hair cells of the inner ear in a mouse model of congenital genetic sensorineural hearing loss using an *in utero*, virus-mediated gene therapy approach. The results of this study provide an exciting and significant step toward the treatment of congenital hearing loss, a step that addresses the underlying cause of deafness.

shown that Msr deficiency leads to various oxidative stress-related disorders, such as neurodegenerative diseases, cystic fibrosis, and aging (1, 8, 12, 24, 32, 35–37). However, until now, the congenital hearing loss that results from a genetic defect in the methionine sulfoxide reductase B3 (*MSRB3*) gene in humans had been considered a unique monogenic disease. Ahmed *et al.* reported that the *MSRB3* gene is associated with human DFNB74, which is a locus for autosomal recessive nonsyndromic hearing loss (1). They identified two mutations, p.Cys89Gly and p.Arg19X, in eight Pakistani families and demonstrated that these mutations result in the loss of MSRB3 enzymatic activity (1). We previously generated an *MsrB3* knockout mouse model ($MsrB3^{-/-}$) and identified a profound hearing loss phenotype that was similar to that observed in hearing loss patients with the *MSRB3* mutations (24). Moreover, we determined that MsrB3 is highly expressed in hair cells, which are the auditory sensory receptors that serve as the key element of sound transduction. We also showed that MsrB3 deficiency results in the degeneration of stereociliary bundles, which is then followed by hair cell apoptosis (24).

Within the inner ear, the cochlea contains the organ of Corti, which is the receptor organ for hearing. Damage to the hair cells of the human cochlea by genetic or environmental factors results in irreversible hearing loss because mammals cannot regenerate hair cells (52). The inability to regenerate hair cells causes sensorineural hearing loss (SNHL), which results from functional abnormalities in the hair cells of the organ of Corti or in auditory nerve cells and accounts for $\sim$90% of hearing loss cases (9–11, 13, 19, 39, 43).

Recently, several groups have reported the results of gene therapy studies that involved therapeutic gene transfer into the cochleae of rodents (2, 3, 31, 55). These studies demonstrated the potential of this therapeutic modality for the treatment of SNHL caused by genetic mutations (2, 3, 31, 55). This approach appears most promising as a means to replace nonfunctional gene products *via* the delivery of functional copies of the affected gene (*e.g.*, complementary DNA; cDNA) in SNHL patients who suffer from nonsyndromic deafness with an autosomal recessive inheritance pattern. To successfully treat this category of patients *via* a gene therapy approach, the exogenously delivered gene should be expressed before the onset of hearing loss. Because the majority of these patients are profoundly deaf from birth, it is reasonable to choose an administration time that corresponds to early inner ear development in the embryo. Bedrosian *et al.* and others demonstrated that *in utero* gene transfer of recombinant adeno-associated virus (rAAV) vectors into the mouse otocyst at embryonic day (E) 12–12.5 was a safe and effective way of targeting sensory hair cell progenitors in the developing cochlea (4, 51). However, there have been no *in vivo* demonstrations that *in utero* gene therapy using rAAVs can rescue hearing function in an animal model with a profound, human-like SNHL phenotype.

In the present study, we applied gene therapy by administering the rAAV that expresses the *MsrB3* gene into the embryonic otocyst of $MsrB3^{-/-}$mice *via* transuterine microinjection. We examined the results of this *in vivo* approach on the hair cell morphology and hearing of these animals.

Results

Validation of rAAV-mediated gene delivery into the cochlea via *a transuterine approach*

To evaluate the safety and feasibility of rAAV injection into the cochlea *via* a transuterine approach, we delivered rAAV2/1-*GFP* directly into the otocyst of $MsrB3^{+/+}$ mice at E12.5 (Supplementary Fig. S1; Supplementary Data are available online at www.liebertpub.com/ars). We then measured auditory brainstem response (ABR) thresholds in both ears of the treated mice at postnatal day (P) 28 to identify any ototoxicity inherent to the procedure. The average ABR thresholds for click stimuli were 19.2, 20.8, and 20 dB in the untreated ear, operated left ear, and contralateral right ear, respectively, of $MsrB3^{+/+}$ mice (Fig. 1A). No significant differences in auditory function were observed between the operated ear and the contralateral ear or between the operated ears and the ears of $MsrB3^{+/+}$ mice ($n=6$ for each group, $p>0.5$; Fig. 1B). Symptoms of vestibular dysfunction that could have been caused by surgical damage, such as circling and head tossing, were not observed (data not shown).

Next, we delivered rAAV2/1-*MsrB3-GFP* into the otocysts of $MsrB3^{+/+}$ mice (Supplementary Fig. S1A) and observed strong green fluorescent protein (GFP) expression in the organ of Corti at P0 (Fig. 2A). Additionally, whole-mount immunostaining of the sensory epithelium revealed that the transduction efficiency was high, as indicated by the high level of GFP expression in >90% and 83% of the inner hair cells (IHCs) and outer hair cells (OHCs), respectively, at P28 ($n=4$ for each group, Fig. 2B, C).

Hearing restoration in $MsrB3^{-/-}$ *mice after delivery of rAAV2/1-MsrB3-GFP into the otocyst*

Because virus-mediated gene delivery into the otocyst did not damage the cochlea and successfully induced transgene expression in hair cells, in which the *MsrB3* gene is normally expressed, we investigated whether virus-mediated expression of the *MsrB3* gene restored hearing function.

To determine whether virus-mediated expression of the *MsrB3* gene restored hearing function, we injected rAAV2/1-*MsrB3-GFP* into the otocyst of $MsrB3^{-/-}$ mice at E12.5 using the transuterine approach. We then measured ABR thresholds when the mice were 4 weeks old (Fig. 3). The ears of untreated and rAAV2/1-*GFP*-treated $MsrB3^{-/-}$ mice did not exhibit responses to click stimuli or tone bursts, which is consistent with the previously reported phenotype of the $MsrB3^{-/-}$ mouse (24) (Fig. 3A, middle panels). In contrast, the treated ear that was injected with the *MsrB3* gene exhibited waveforms that were

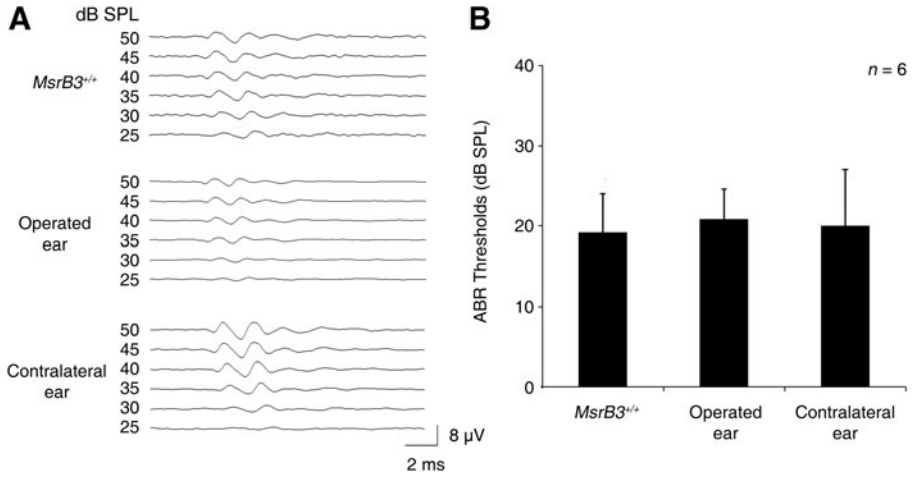

FIG. 1. Auditory function following transuterine rAAV-mediated gene delivery in *MsrB3*$^{+/+}$ mice. (A) Click-evoked ABR response of an untreated ear (*upper*), an operated ear (*middle*), and a contralateral ear (*lower*) of an *MsrB3*$^{+/+}$ mouse at P28 after administration of the rAAV2/1-*GFP* treatment. The amplitude of the response is measured in microvolts (μV). The time is expressed in milliseconds (ms) and is indicated on the *x*-axis. **(B)** The average click-evoked ABR thresholds of each group are shown. No significant differences were observed between the groups ($n=6$ for each group, $p>0.5$). Student's *t*-tests were conducted for statistical comparisons. The data are shown as the mean ± SD. ABR, auditory brainstem response; GFP, green fluorescent protein; MsrB3, methionine sulfoxide reductase B3; rAAV, recombinant adeno-associated virus.

typical of a normal hearing threshold and that were similar to those observed in *MsrB3*$^{+/+}$ mice (Fig. 3A, left and right panel). At all frequencies measured, ABR thresholds differed significantly between the ears of the rAAV2/1-*GFP*-treated *MsrB3*$^{-/-}$ mice and those treated with rAAV2/1-*MsrB3-GFP*, whereas at 16 and 32 kHz, there was a slight distinction between the ears of the *MsrB3*$^{+/+}$ mice and those of *MsrB3*$^{-/-}$ mice that were treated with rAAV2/1-*MsrB3-GFP* ($n=5$ for each group, $^*p<0.05$; Fig. 3B).

Then, we determined the duration of the hearing recovery in the ears of the rescued *MsrB3*$^{-/-}$ mice. In all of the rescued mice, the improved hearing performance was maintained for at least 4 weeks after the treatment. However, hearing thresholds began to deteriorate beginning with the high frequencies at

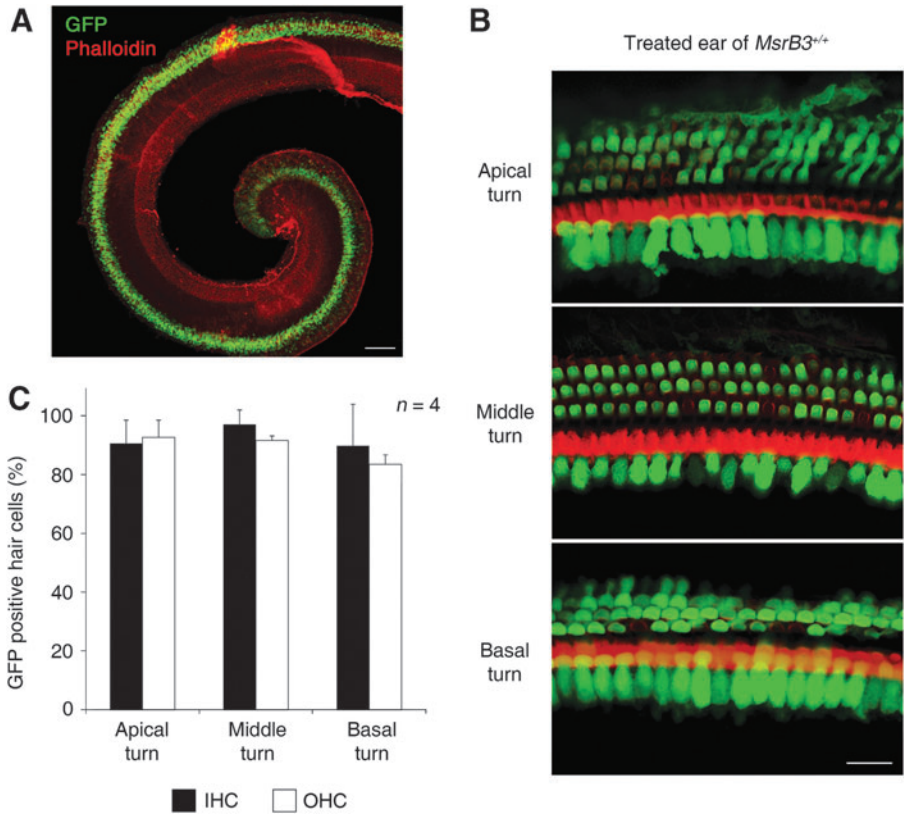

FIG. 2. Expression of GFP in *MsrB3*$^{+/+}$ mice following rAAV-mediated gene transfer into the organ of Corti. (A) Immunostaining was performed to detect rAAV-transduced cells. Fluorescence images show the organ of Corti from an *MsrB3*$^{+/+}$ mouse that is immunostained for GFP (*green*) and phalloidin (*red*) at P0. **(B)** Fluorescence images show that the GFP-positive cells consisted primarily of IHCs and OHCs at P28. **(C)** The graph represents the transduction efficiency of IHCs and OHCs in each of the three turns, the apical, middle, and basal turns, within a 160-μm region of the organ of Corti. No significant differences were observed between the groups ($p>0.1$, $n=4$ for each group). Student's *t*-tests were conducted for statistical comparisons. The data are shown as the mean ± SD. IHC, inner hair cell; OHC, outer hair cell. Scale bars: 20 μm.

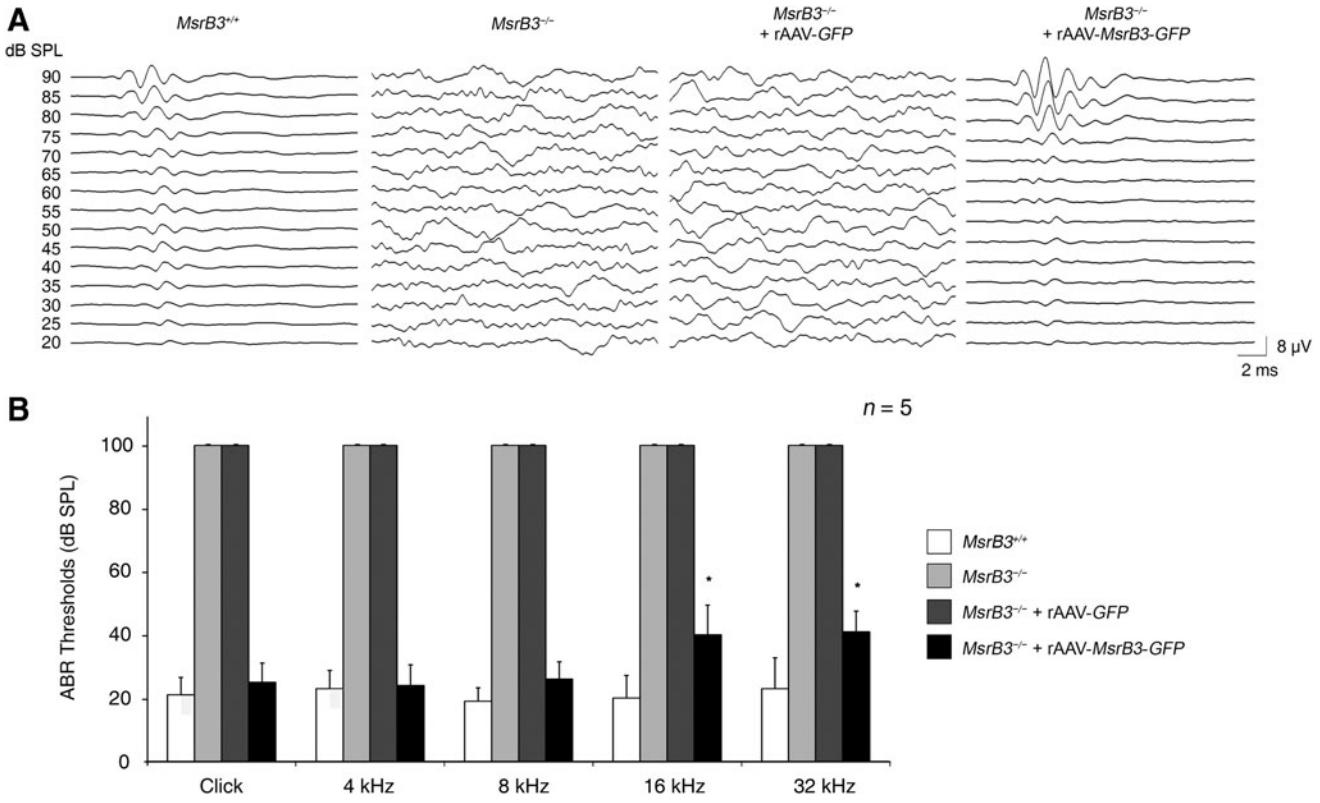

FIG. 3. Restoration of auditory function following rAAV2/1-mediated *MsrB3* gene transfer into the otocysts of *MsrB*$^{-/-}$ mice. (A) Example of click-evoked ABR response of a post-treatment *MsrB3*$^{-/-}$ mouse ear compared with that of an *MsrB3*$^{+/+}$ mouse ear at P28. The waveform of the rAAV2/1-*MsrB3-GFP*-treated ear was changed after treatment. **(B)** Graphical representation of the ABR data that show the average ABR thresholds for click and tone burst (4, 8, 16, and 32 kHz) stimuli of the five rescued *MsrB3*$^{-/-}$ mice. *Asterisks* indicate statistical differences between the ears of the *MsrB3*$^{+/+}$ mice and the rAAV2/1-*MsrB3-GFP*-treated ears of the *MsrB3*$^{-/-}$ mice ($*p < 0.05$). *p*-Values were determined by Student's *t*-tests. The data are shown as the mean ± SD. $n = 5$ for each group.

~7 weeks of age, and the reduced hearing function remained at 8 weeks after treatment (Supplementary Fig. S2A).

Exogenous expression of MsrB3 *in the inner ear in mice that were injected with rAAV2/1-MsrB3-GFP into the otocyst*

To investigate whether the hearing restoration resulted from the delivery of the *MsrB3* gene, we next performed histological analyses of the rescued *MsrB3*$^{-/-}$ mice (Fig. 4). Whole-mount immunostaining of the ears of *MsrB3*$^{-/-}$ mice that were treated with rAAV2/1-*MsrB3-GFP* was performed at P28 and revealed robust GFP expression in the cells of the organ of Corti (Fig. 4A). The GFP signal was strong in the IHCs and OHCs along the cochlear turns, and the average number of GFP-positive IHCs and OHCs was in the range of 89–91% and 84–92%, respectively ($n = 4$ for each group, Fig. 4B), indicating a similar level of transduction efficiency as that observed in the rAAV2/1-*MsrB3-GFP*-injected *MsrB3*$^{+/+}$ mice.

Then, we confirmed expression of the MsrB3 and of GFP in the ears of the rescued *MsrB3*$^{-/-}$ mice because the expression of these genes was driven by individual cytomegalovirus (CMV) promoters within the same rAAV2/1 backbone. As shown in Figure 4C, expression of the MsrB3 and of GFP was specifically observed in both types of hair cells within the cochlea. The expression was also largely overlapping within the IHCs and OHCs, indicating successful rAAV-mediated transgene delivery into the hair cells of the rescued *MsrB3*$^{-/-}$ mice.

We also used reverse transcription–polymerase chain reaction (RT-PCR) to examine the mRNA expression levels of the transduced *MsrB3* gene in the ears of *MsrB3*$^{-/-}$ mice that were treated with rAAV2/1-*MsrB3-GFP* (Fig. 5A). Compared with rAAV2/1-*GFP*-treated ears and the untreated ears of *MsrB3*$^{-/-}$ mice, the ears of the *MsrB3*$^{-/-}$ mice that were treated with rAAV2/1-*MsrB3-GFP* exhibited some *MsrB3* expression, but the expression level was lower than that observed in *MsrB3*$^{+/+}$ mice. This result confirmed that the *MsrB3* gene was introduced into the cochlea and properly expressed in the *MsrB3*$^{-/-}$ mice and that this expression was associated with the restoration of hearing function.

To quantify the level of MsrB3 protein that was produced following delivery of the viral vector, we performed a Western blot analysis of inner ear protein extracts from *MsrB3*$^{+/+}$ mice, *MsrB3*$^{+/-}$ mice, and *MsrB3*$^{-/-}$ mice that were treated with rAAV2/1-*MsrB3-GFP* and untreated *MsrB3*$^{-/-}$ mice (Fig. 5B). The level of MsrB3 protein in the inner ears of the *MsrB3*$^{+/-}$ mice was 43 ± 4.2% of the level observed in the *MsrB3*$^{+/+}$ mice. Moreover, MsrB3 was not expressed in the inner ears of the untreated *MsrB3*$^{-/-}$ mice (Fig. 5C). Strikingly, the level of MsrB3 protein expression in the inner

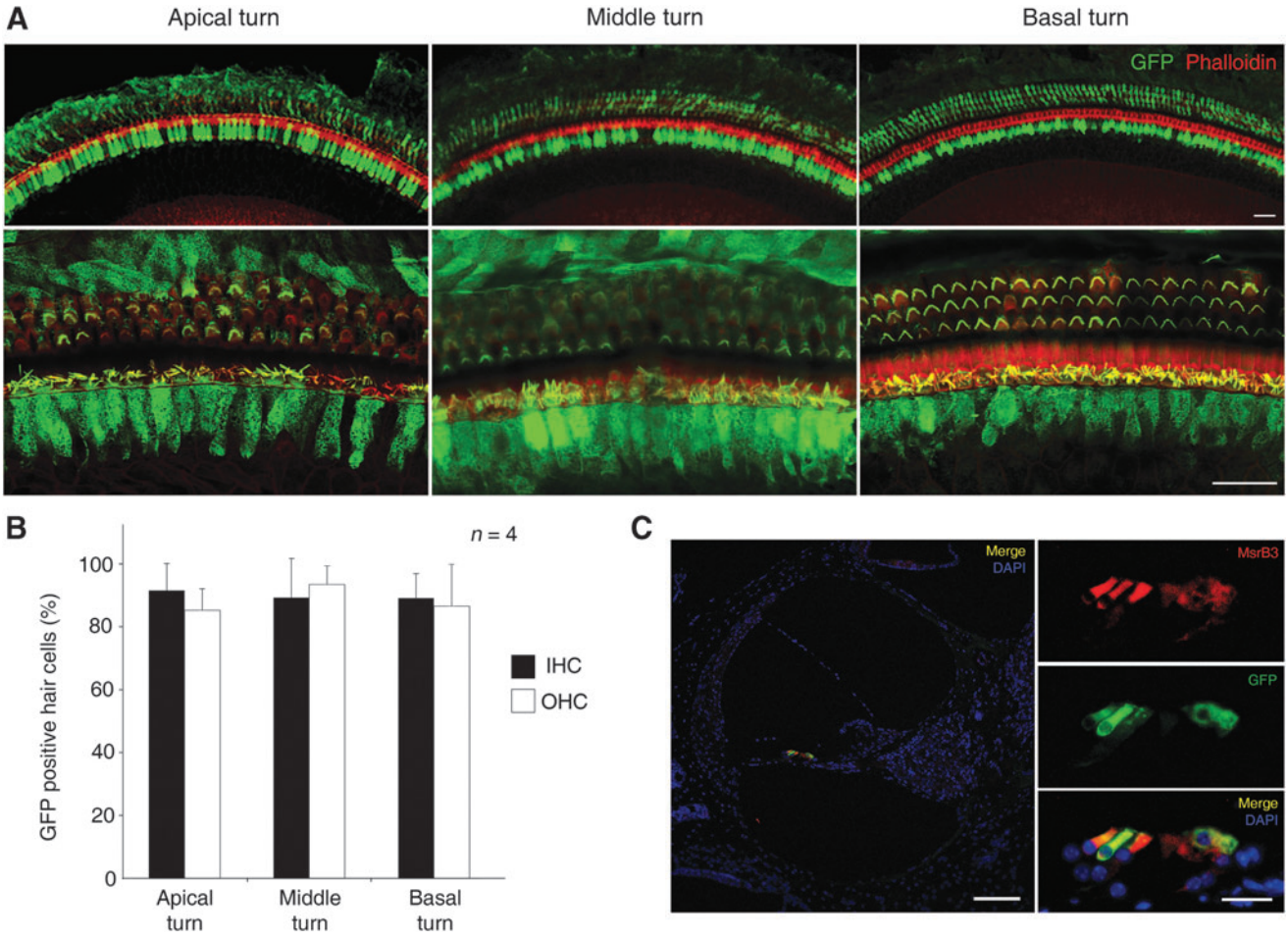

FIG. 4. Localization and transduction efficiency of MsrB3 and GFP following gene transfer. (A) An anti-GFP antibody was used to label the organ of Corti of the treated left ears of 28-day-old *MsrB3*$^{-/-}$ mice, and F-actin was labeled using Alexa 555-conjugated phalloidin. The tissue samples were then imaged with a fluorescence microscope. The low-magnification images show the distribution of GFP expression following the delivery of rAAV2/1-*MsrB3-GFP* into the otocysts of *MsrB3*$^{-/-}$ mice (*upper panel*). The high-magnification images show that GFP (*green*) was detected in both the IHCs and OHCs (*lower panel*) in the rescued *MsrB3*$^{-/-}$ mice. **(B)** Graphical representation of the percentage of GFP-positive cells that were transfected with rAAV2/1-*MsrB3-GFP* within a 160-μm region of IHCs and OHCs in each of the three turns, including the apical, middle, and basal turn. No significant differences were observed between the groups ($p > 0.05$, $n = 4$ for each group). *p*-Values were determined by Student's *t*-tests. The data are shown as the mean ± SD. **(C)** MsrB3 and GFP were specifically expressed in both types of hair cells within the cochlea (*left panel*). The higher-resolution images show that MsrB3 and GFP were colocalized in both the IHCs and OHCs in the organ of Corti (*right panel*). The scale bars represent 25 μm in **(A)**, 100 μm in **(C**, *left panel***)**, and 20 μm in **(C**, *right panel***)**.

ears of the rescued *MsrB3*$^{-/-}$ mice was found to be 15 ± 1.6% of that observed in the *MsrB3*$^{+/+}$ mice.

Taken together, our results demonstrate that delivery of the *MsrB3* gene *via* transuterine injection of a viral vector successfully produced stable expression of the transgene in the targeted area (*i.e.*, hair cells at an early developmental stage) and that this expression ultimately rescued the hearing of the *MsrB3*$^{-/-}$ mice.

Localization of the exogenous MsrB3 *gene within the organ of Corti of the rescued* MsrB3$^{-/-}$ *mice*

To compare the distribution of exogenous MsrB3 delivered by rAAV2/1 with that of endogenous MsrB3, at P28, we performed immunohistochemistry on the ears of *MsrB3*$^{+/+}$ mice as well as on the ears of untreated *MsrB3*$^{-/-}$ mice, *MsrB3*$^{-/-}$ mice that were treated with rAAV2/1-*GFP*, and *MsrB3*$^{-/-}$ mice that were treated with rAAV2/1-*MsrB3-GFP* (Fig. 6). We immunohistochemically detected Myo7a using a green label. The GFP signal was not confused with the green label for Myo7a because following AAV viral infection, the GFP signal was not detected in paraffin-embedded sections without antibody enhancement even though GFP was coexpressed with MsrB3. MsrB3 expression was localized in both IHCs and OHCs and was colocalized with Myo7a expression in the ears of the *MsrB3*$^{-/-}$ mice that were treated with rAAV2/1-*MsrB3-GFP*; this pattern was similar to that observed in the ears of the *MsrB3*$^{+/+}$ mice (Fig. 6A–C, J–L), although endogenous MsrB3 is more broadly expressed, including from the inner sulcus cells to the outer sulcus cells (24). MsrB3 expression was not observed in the untreated ears or rAAV2/1-*GFP*-treated ears of *MsrB3*$^{-/-}$ mice

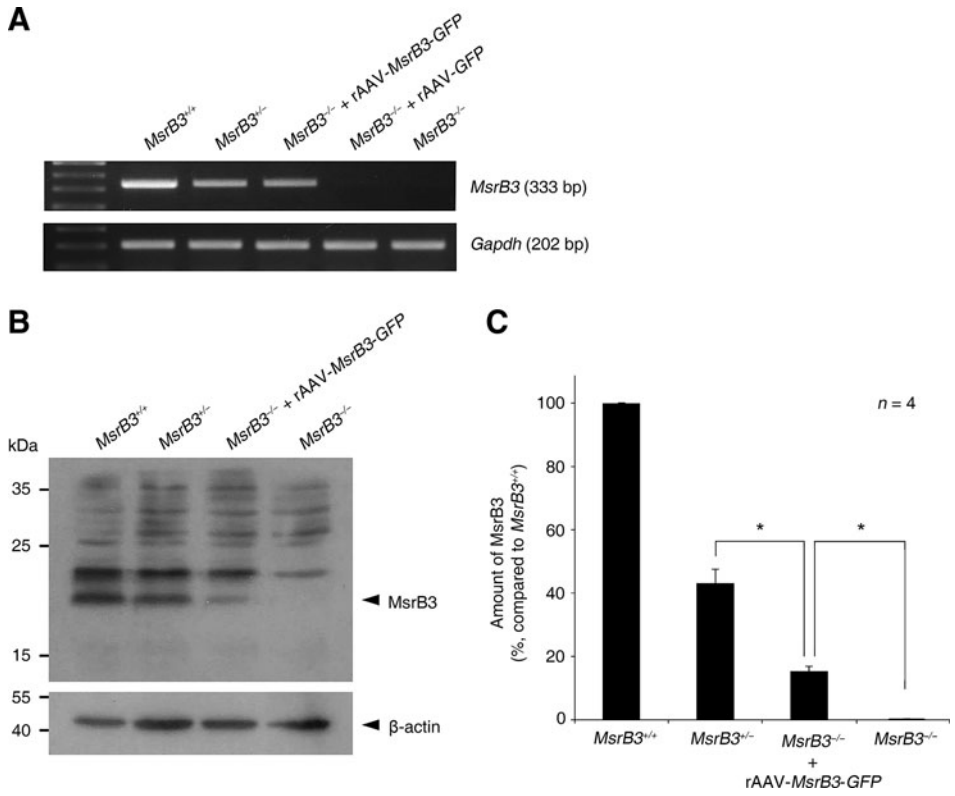

FIG. 5. Quantification of exogenous MsrB3 expression levels using RT-PCR and Western blot analysis. (A) RT-PCR analysis of *MsrB3* expression, which confirmed the success of rAAV-mediated gene transfer. Total RNA was extracted from the inner ears of $MsrB3^{+/+}$ and rescued $MsrB3^{-/-}$ mice at P28. *MsrB3* mRNA was found in the ears of the $MsrB3^{+/+}$ mice and $MsrB3^{+/-}$ mice and in the rAAV2/1-*MsrB3-GFP*-treated ears of the $MsrB3^{-/-}$ mice. *Gapdh* served as an internal control. **(B)** Western blot analysis of inner ears extracted from $MsrB3^{+/+}$ mice, $MsrB3^{+/-}$ mice, the rescued ears of $MsrB3^{-/-}$ mice, and the untreated ears of $MsrB3^{-/-}$ mice at P28. β-actin was used as a quantitative loading control. MsrB3 protein was also detected in the rescued ears of the $MsrB3^{-/-}$ mice. **(C)** Graphical representation of the relative MsrB3 levels, which were normalized to β-actin, in the ears of $MsrB3^{+/-}$ mice and in the rAAV2/1-*MsrB3-GFP*-treated and untreated ears of $MsrB3^{-/-}$ mice compared with those in the ears of $MsrB3^{+/+}$ mice. *Asterisks* denote significant differences between the rAAV2/1-*MsrB3-GFP*-treated ears of the $MsrB3^{-/-}$ mice and the untreated ears of $MsrB3^{+/-}$ or $MsrB3^{-/-}$ mice ($n = 4$ for each group, $^*p < 0.001$). *p*-Values were determined by Student's *t*-tests. The data are shown as the mean ± SD. GAPDH, glyceraldehyde-3-phosphate dehydrogenase; RT-PCR, reverse transcription–polymerase chain reaction.

(Fig. 6D–I). These results demonstrate that delivery of the exogenous *MsrB3* gene at E12.5 successfully targeted expression to both the IHCs and OHCs of the organ of Corti in the ears of the rescued $MsrB3^{-/-}$ mice that were treated with rAAV2/1-*MsrB3-GFP*.

Ultrastructure of stereociliary bundles in the IHCs and OHCs of the rescued MsrB3$^{-/-}$ *mice*

In a previous study, we demonstrated that $MsrB3^{-/-}$mice exhibit progressive degeneration of stereociliary bundles starting at P8 and that this degeneration is followed by a loss of hair cells that results in profound deafness (24). Therefore, we assessed morphological rescue of the stereociliary bundles in the ears of the rescued $MsrB3^{-/-}$ mice at the ultrastructural level using scanning electron microscopy (SEM; Fig. 7). In the organ of Corti of 28-day-old $MsrB3^{+/+}$ mice, the stereociliary bundles of the IHCs exhibited a normal approximately linear shape, and those of the OHCs exhibited a V-like shape, consistent with our previous results (Fig. 7A, left column). Degeneration of the stereociliary bundles of both OHCs and IHCs was observable at P28 in the ears of $MsrB3^{-/-}$ mice compared with those of $MsrB3^{+/+}$ mice (Fig. 7A, middle column). The stereociliary bundles in the ears of the rescued $MsrB3^{-/-}$ mice, in which the *MsrB3* gene was delivered into the otocyst, exhibited OHC and IHC morphologies that were similar to those of the $MsrB3^{+/+}$ mice (Fig. 7A, right column). Previous studies have reported that more severe hair cell degeneration appears in the apical turn than in the middle and basal turns in $MsrB3^{-/-}$ mice. Magnified views of the stereociliary bundles indicated that the structure of OHCs and IHCs was similar throughout all cochlear turns in the ears of the rescued $MsrB3^{-/-}$ mice, similar to the $MsrB3^{+/+}$ mice (Fig. 7B). However, at 5 weeks of age, stereociliary bundle degeneration was observed in all of the cochlear turns, and this degeneration was more severe at 7 weeks of age (Supplementary Fig. S2B). This observation correlated with the progressive loss of hearing ability in the rescued ears of the $MsrB3^{-/-}$ mice (Supplementary Fig. S2). Overall, our results indicate that hearing function recovered due to restoration of the stereociliary bundles of hair cells in the treated ears of the rescued $MsrB3^{-/-}$ mice until 4 weeks of age and that both hearing ability and the morphological integrity of the stereociliary bundles deteriorated after 4 weeks of age.

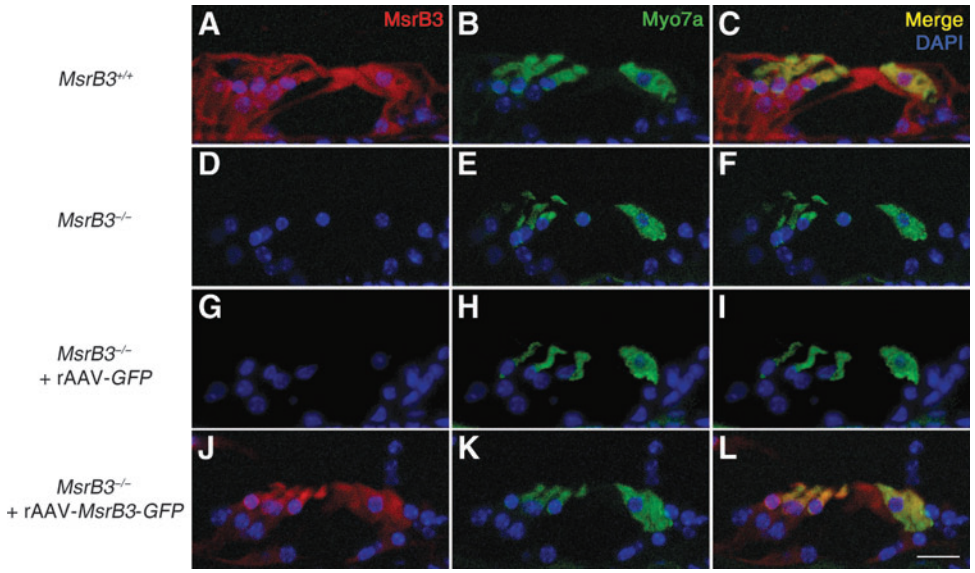

FIG. 6. Immunohistochemical analysis of MsrB3 expression in cochlear sections. Immunohistochemistry was performed on serially sliced inner ear samples from the ears of *MsrB3*$^{+/+}$ mice and from the untreated, rAAV2/1-*GFP*-treated, and rAAV2/1-*MsrB3-GFP*-treated ears of *MsrB3*$^{-/-}$ mice at P28. The expression of MsrB3 protein (*red*) and Myo7a (*green*) was assessed in *MsrB3*$^{+/+}$ mice **(A–C)**. No MsrB3 expression was found in the untreated ears or rAAV2/1-*GFP*-treated ears of the *MsrB3*$^{-/-}$ mice **(D–I)**. In contrast, the rescued ears of the *MsrB3*$^{-/-}$ mice exhibited local expression of exogenous MsrB3 in the IHCs and OHCs, and the expression of exogenous MsrB3 overlapped with that of Myo7a **(J–L)**. Scale bars represent 10 μm.

Discussion

SNHL is the most common type of hearing loss in humans, and in >50% of all newborns with SNHL, the hearing loss is caused by genetic factors. However, there are no fundamental therapies to correct the underlying cellular deficit in these cases. To date, the hearing loss is managed by providing patients with appropriate amplification systems, such as hearing aids or cochlear implants. Currently, cochlear implantation (CI) is the only effective treatment option for profound deafness (10, 30, 31, 40). However, CI has many drawbacks, including the surgical burden, the variable auditory outcome, and the inherent problems of implantable devices.

Advances in gene therapy that would enable the regeneration of hair cells or the restoration of auditory function have been considered as a promising way to improve therapies for hearing restoration in a clinical setting (www.wiley.co.uk/genmed/clinical); nevertheless, few studies have reported positive gene therapy results for hearing loss (2, 31). Miwa *et al.* reported that supplemental expression of the connexin 30 (Cx30)-encoding gene *via* its electroporation into the otocyst during the embryonic stage could ameliorate deafness caused by the loss of Cx30 expression (31). However, in practice, critical obstacles, such as surgical damage and low expression efficiency, preclude clinical application of electroporation-based gene transfer to the otocyst. Akil *et al.* demonstrated the restoration of hearing in vesicular glutamate transporter 3 (*Vglut3*) knockout mice after reinsertion of the *Vglut3* gene using rAAV-mediated transfer during the postnatal period, suggesting a potential treatment option for genetic forms of hearing loss (2). However, newborns are able to hear, indicating that the functional and anatomical development of the human ear is largely complete at birth. Therefore, treatments for congenital hearing loss in humans should ideally be targeted to the embryonic period.

In this study, we demonstrated that delivery of rAAV2/1-*GFP* into the otocyst at E12.5 led to high transduction efficiency, as demonstrated by GFP expression, in cells in the organ of Corti, including IHCs, OHCs, and supporting cells, similar to previous reports (20, 21). Therefore, rAAV2/1-mediated gene delivery could be a useful therapeutic approach for hearing loss that results directly from hair cell defects.

We also showed that a single transuterine injection of rAAV2/1-*MsrB3-GFP* was sufficient to restore hearing in *MsrB3*$^{-/-}$ mice based on ABR and histological studies. The improvement of ABR thresholds that was observed in the rAAV2/1-*MsrB3-GFP*-treated ears compared with the untreated ears of the *MsrB3*$^{-/-}$ mice persisted for at least 4 weeks after birth. This functional recovery correlated with the levels of exogenous *MsrB3* transcript and protein, as demonstrated by RT-PCR and Western blot analyses, respectively. Interestingly, the level of exogenous MsrB3 protein in the rescued ears of the *MsrB3*$^{-/-}$ mice was only $\sim$15% that observed in the ears of the *MsrB3*$^{+/+}$ mice, but this level was sufficient to rescue hearing function. These results are consistent with the results of a previous rAAV-mediated gene therapy study that demonstrated that $\sim$15% of the normal level of phosphodiesterase expression was sufficient to prevent retinal degeneration in mice (38). Additionally, Lee *et al.* reported that heterozygous or homozygous patients who harbored the c.919-2A>G splice mutation in the *SLC26A4* gene exhibited better residual hearing compared with those who carried the missense mutation, p.H723R, which is the most common cause of hearing loss (28). A residual level of normal mRNA (6–17%) is thought to be the underlying cause of the better hearing abilities of patients with splice mutations compared with missense mutations. Together, these results suggest that a low level of gene expression is sufficient to restore some degree of function in recessive hereditary disorders that are characterized by loss-of-function pathogenicity.

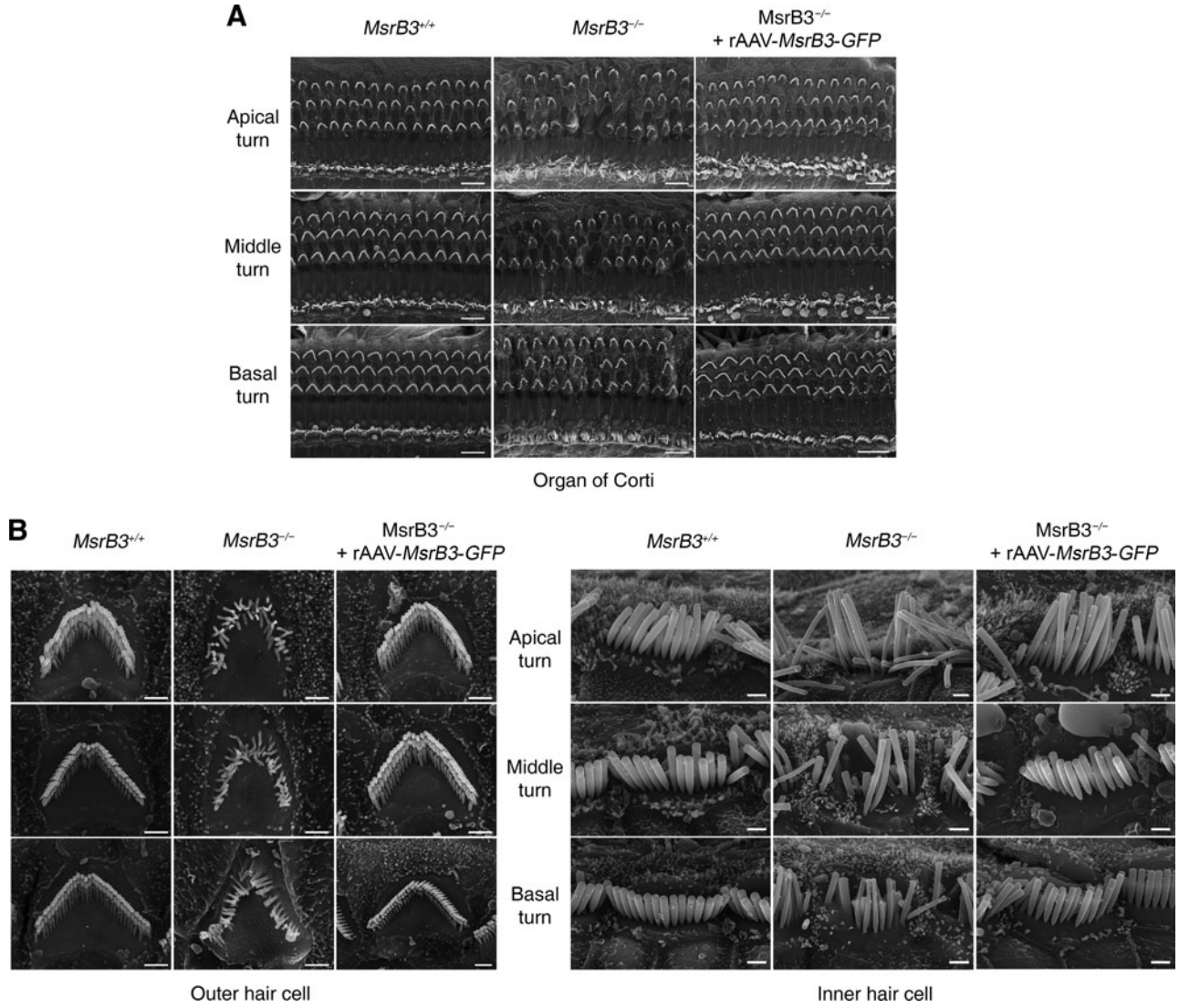

FIG. 7. Ultrastructural morphology of the stereociliary bundles. *MsrB3*$^{+/+}$, *MsrB3*$^{-/-}$, and rescued *MsrB3*$^{-/-}$ mice were sacrificed at P28 for scanning electron microscopy analysis. The images show stereociliary bundles along the three cochlear turns, including the apical, middle, and basal turn. **(A)** Overview image of a large portion of the organ of Corti that shows the stereociliary bundles of the three *rows* of OHCs and one *row* of IHCs in the ears of *MsrB3*$^{+/+}$ (*left column*) mice, the ears of *MsrB3*$^{-/-}$ mice (*middle column*), and the ears of rescued *MsrB3*$^{-/-}$ mice (*right column*). **(B)** Representative higher-resolution images of the OHCs (*left panel*) and IHCs (*right panel*). IHC, inner hair cell; OHC, outer hair cell. The scale bars represent 10 μm in **(A)** and 1 μm in **(B)**.

We also observed that the morphology of the stereociliary bundles in the rescued ears was close to normal and that this largely normal morphology was maintained at P28. Because we previously demonstrated that the stereociliary bundles of hair cells in the apical turn were more severely degenerated than those in the other turns in *MsrB3*$^{-/-}$ mice, we assessed the extent of the rescue of the stereociliary bundles along the cochlear turns in the rescued ears. Interestingly, the stereociliary bundles of the hair cells in all of the cochlear turns of the rescued ears of the *MsrB3*$^{-/-}$ mice were shaped normally and appeared similar to those in the *MsrB3*$^{+/+}$ mice. Additionally, we consistently observed the preferential expression of rAAV2/1 toward the cochlear apical turn, although all turns exhibited high transduction efficiency. This result suggests that elevated expression of exogenous MsrB3 in the cochlear apical turn may have further supported the formation of normal stereociliary bundles, and this expression pattern could explain why threshold improvements for low frequencies persisted longer than those for high frequencies in the rescued ears of the *MsrB3*$^{-/-}$ mice.

In a previous report, we identified that *MsrB3* is important for the maintenance of hair cells rather than for their differentiation or development, suggesting that the degeneration of stereociliary bundles in hair cells is the primary cause of the hearing loss that resulted from the absence of MsrB3 enzymatic activity in the *MsrB3*$^{-/-}$ mice (24). Although the precise pathogenic mechanism by which MsrB3 deficiency results in hearing loss and the specific target proteins that are reduced by the MsrB3 enzyme have not yet been identified, we speculate that the accumulation of oxidative stress is not the major cause of MsrB3 deficiency-induced hair cell degeneration; instead, the failure of redox regulation of specific

target proteins in the hair cell is a primary factor as demonstrated by the absence of significant differences in MsrB enzyme activity and carbonylated protein levels between the inner ears of *MsrB3*$^{-/-}$ and *MsrB3*$^{+/+}$ mice. Additionally, the *MsrB3*$^{-/-}$ mice showed more severe hair cell defects in the apical turn of the cochlea. This pattern of defects is in contrast with the general characteristics of oxidative stress-mediated hearing loss, which predominantly affects the hair cells in the basal turn of the cochlea (24). Redox regulation provides signals that are necessary for important cellular processes, such as immune responses, hormone synthesis, Ca^{2+} homeostasis, and cytoskeletal remodeling, among others (54). We focused on studies of redox balance regulation of actin dynamics because actin dynamics play an essential role in the stereociliary bundles of hair cells. Recently, Hung *et al.* showed that the monooxygenase, Mical, acts as an actin regulator by inducing the disassembly of F-actin *via* the selective oxidization of two Mets (the 44th and 47th Met, residue numbers from rabbit) of F-actin (15, 16). Lee *et al.* followed up this study by demonstrating that MsrB1 and MsrB2 reduce the oxidized Mets in Mical-treated F-actin and therefore act as Mical antagonists in the control of actin disassembly and assembly (27). Interestingly, MsrB3 is localized at the base of the stereocilia, suggesting that MsrB3 may act as a regulator of actin dynamics (24). Based on these reports, we propose that MsrB3 deficiency may result in the accumulation of oxidized Met and induce the disassembly of F-actin and stereocilia degeneration in the hair cells of *MsrB3*$^{-/-}$ mice. In addition, the role of MsrB3 in supporting cells and the role of potassium and magnesium channels, which are known to be regulated by Met redox signaling (6, 7, 14, 42), should also be considered in further studies to more fully understand *MsrB3*-related hearing loss and to enable the development of improved therapies for *MsrB3* deficiency.

In this study, our findings demonstrated that the restoration of the stereociliary bundles of hair cells and of hearing function in the *MsrB3*$^{-/-}$ mice resulted from successful *MsrB3* gene transfer into the otocyst. However, this study had several limitations. First, the rescued hearing loss in the rAAV2/1-*MsrB3-GFP*-treated ears of the *MsrB3*$^{-/-}$ mice persisted for 4 weeks after birth, but hearing subsequently deteriorated, and the deterioration of hearing also correlated with the degeneration of hair cell stereociliary bundles. Similar variability in the duration of post-treatment hearing restoration was also reported by Akil *et al.*, who found that a variable level of hearing loss developed after 7 weeks in knockout mice that were rescued by rAAV-mediated gene therapy (2). There are several potential explanations for why the hearing ability of the rescued mice did not persist. However, we can rule out an influence of either treatment time or delivery approach on the hearing loss variability because our studies and the study of Akil *et al.* used different time points of treatment (embryonic *vs.* postnatal) and delivery techniques (transuterine *vs.* cochleostomy and injection through the round window membrane). One possible explanation for the variability in the duration of post-treatment hearing restoration is the tropism of the rAAV serotype used in the gene therapy. Studies by us and others have shown that rAAV2/1 is the most suitable serotype to use as a delivery vector when targeting hair cells in gene therapies for SNHL (4, 51). When we analyzed the localization of MsrB3, we observed a small difference in the expression pattern of MsrB3 in the inner ear between the ears of the rescued *MsrB3*$^{-/-}$ mice and the ears of *MsrB3*$^{+/+}$ mice. Indeed, MsrB3 expression was restricted to the hair cells and was rarely observed in the supporting cells of the treated ears. Therefore, we hypothesize that although hearing was rescued during the early postnatal period when MsrB3 expression was localized to the inner ear hair cells, more widespread expression of MsrB3 might be necessary to maintain hearing in the adult mouse inner ear. To overcome this variability, (1) it may be necessary to treat with a combination of different rAAV serotypes to target different type of cells in the cochlea and (2) readministration of rAAV in treated *MsrB3*$^{-/-}$ mice during the early postnatal period may also improve the therapeutic stability of the hearing restoration. Second, the study included the limitations that are inherent to the *in utero* gene delivery method in terms of clinical application. Further studies are required to develop a suitable method for *in utero* gene delivery in humans. However, our study demonstrates that rAAV-mediated gene therapy could be a promising strategy for rescuing the function of the sensory hair cells of the mammalian inner ear in hereditary deafness.

In summary, to our knowledge, this is the first study to demonstrate functional and morphological rescue of the hair cells of the inner ear in a mouse model of congenital SNHL caused by a deafness gene using an *in utero* rAAV-mediated gene therapy strategy. Although further studies of the maintenance of the restored hearing function and the development of methods to apply gene therapy in humans are needed, there is no doubt that our study has led patients with sensorineural deafness one step closer toward the restoration of hearing function.

Materials and Methods

Recombinant adeno-associated virus

All of the rAAVs used in this study contained the inverted terminal repeat of AAV serotype 2 and the capsid of AAV serotype 1 (rAAV2/1) and were purchased from SignaGen Laboratories (Rockville, MD). Prepackaged rAAVs were used that contained either a *GFP* gene (rAAV2/1-*GFP*), driven by a CMV or CMV early enhancer/chicken β-actin (CAG) promoter, or a mouse *MsrB3* cDNA along with GFP (rAAV2/1-*MsrB3-GFP*), driven by the CMV promoter (Supplementary Fig. S1A). In this study, the rAAV titers were defined as vector genome copies per milliliter (VG/ml). The titer of the rAAV2/1-CAG-*GFP* stock was 1.2×10^{13} VG/ml, and the titers of both the rAAV2/1-CMV-*GFP* and rAAV2/1-*MsrB3-GFP* stocks were 1.31×10^{13} VG/ml. The rAAVs were stored at −80°C and thawed immediately before the surgery.

Animals

Pregnant females of the Institute for Cancer Research (ICR) strain (12–14 weeks of age) were purchased from Hyochang Science (Daegu, Republic of Korea) and used as wild-type (WT) controls to validate the safety and efficiency of rAAV2/1-*GFP*- and rAAV2/1-*MsrB3-GFP*-mediated gene delivery into the otocyst at E12.5. *MsrB3*$^{-/-}$ mice were used for rAAV-mediated gene transfer of the *MsrB3* gene. Details regarding the *MsrB3*$^{-/-}$ mice have been published elsewhere (24).

Surgical procedures

All surgical procedures were performed on a dedicated surgical work surface using sterile techniques. Pregnant ICR

or *MsrB3*$^{-/-}$ mice were anesthetized at 12.5 days postcoitus by intramuscular (i.m.) injection of tiletamine–zolazepam (1.8 mg/100 g) and xylazine hydrochloride (0.7 mg/100 g) mixtures. After the belly hair was removed from the surgical site, we incised the abdominal skin along the midline over ~15–20 mm. To maintain the body temperature of the pregnant mice, we used a heating pad and infused prewarmed (37°C) normal saline into the abdomen at various times during the surgery. Approximately 0.6–1 μl of rAAV2/1-*GFP* or rAAV2/1-*MsrB3-GFP* was microinjected into the left otocyst (Supplementary Fig. S1B) of the E12.5 embryos using a glass micropipette connected to a 25-μl Hamilton syringe (Hamilton, Bonaduz, Switzerland). The rAAV solution contained fast green FCF dye (Sigma-Aldrich, St. Louis, MO) to accurately visualize the position of the glass micropipette during the injection. The contralateral right otocyst of each embryo served as an internal control because in each embryo, the virus was delivered unilaterally to the left otocyst. After the embryo was injected, we irrigated the abdomen with prewarmed normal saline, closed the abdominal wound with surgical sutures, and covered it with a povidone/iodine-impregnated wound dressing.

Auditory brainstem response measurement

To assess auditory function, we performed ABR measurements using an ABR workstation (System 3; Tucker Davis Technology (TDT), Inc., Alachua, FL) as previously described (29). All tests were conducted in a soundproofed room. Briefly, before ABR measurement, the animals were anesthetized by i.m. injection of tiletamine–zolazepam (1.8 mg/100 g) and xylazine hydrochloride (0.7 mg/100 g) mixtures and placed on a heating pad to maintain their body temperature at 37°C. The animal's body temperature was monitored using a rectal thermometer. To record the ABRs, subcutaneous needle electrodes were inserted into the vertex (+charge), mastoid (−e), and hind leg (ground). Acoustic stimuli consisted of either a tone burst stimulus with a 1-ms rise/fall time and a 5-ms plateau at frequencies of 4, 8, 16, and 32 kHz or transient click stimuli and were applied monaurally through a speaker. The stimulus signals were generated by SigGenRP and an RP2.1 real-time processor, and then transmitted through a programmable attenuator (PA5, TDT), a speaker driver (ED1, TDT), and an electrostatic speaker (EC1, TDT). At every frequency, 500 repetitions of each stimulus were generated, starting from a 90-dB sound pressure level and decreasing in 5-dB steps to the acoustic threshold. The phase of the stimulus was reversed upon each presentation to reduce artifacts caused by repetitive stimuli.

Immunostaining of cochlear whole mounts

The organ of Corti was prepared from the inner ears of the ICR and *MsrB3*$^{-/-}$ mice. The isolated inner ears were quickly fixed by injecting 4% paraformaldehyde (PFA, pH 7.4) in phosphate-buffered saline (PBS) through the oval window, and then immersing them in the same fixative for 2 h at 4°C. After Reissner's membrane and the lateral wall and tectorial membrane of the cochlea were removed, the organ of Corti was dissected into individual turns. The tissues were permeabilized with 0.1% Triton X-100 in PBS (PBS-Tx) for 30 min, blocked using a blocking solution comprising 5% normal goat serum diluted in PBS-Tx for 1 h at room temperature (RT), and stained with either a mouse anti-GFP antibody (1:400; Millipore Filter Corporation, Bedford, MA) or a rabbit anti-MsrB3 antibody (1:200; Sigma-Aldrich) diluted in the blocking solution at 4°C overnight. The next day, the tissue sections were washed with PBS and then incubated for 1 h at RT with an Alexa Fluor 488 (fluorescein)-conjugated goat anti-rabbit IgG secondary antibody (1:1000; Invitrogen, La Jolla, CA) diluted in the blocking solution. Next, F-actin was labeled with an Alexa Fluor® 555-conjugated phalloidin stain (1:1000; Molecular Probes, Eugene, OR) in PBS-Tx for 3 h at RT. The samples were washed with PBS to remove any residual antibodies, mounted with Fluoromount (Sigma-Aldrich), and sealed with a microscope coverslip (Marienfeld Laboratory, Lauda-Königshofen, Germany). The mounted specimens were imaged using a laser scanning confocal microscope (LSM 700; Carl Zeiss, Thornwood, NY). Then, single-transfected IHCs and OHCs were counted in a 160-μm portion of each turn.

RT-PCR analysis

The inner ears were dissected from WT, *MsrB3*$^{-/-}$, and treated *MsrB3*$^{-/-}$ mice. Total RNA was extracted from the whole inner ear using an RNeasy® Micro Kit (Qiagen, Hilden, Germany). We synthesized single-stranded cDNA from the extracted total RNA using the High-Capacity cDNA Reverse Transcription Kit (Applied Biosystems, Foster City, CA). The cDNA samples were used for polymerase chain reaction (PCR) amplification with specific primers for mouse *MsrB3* (NM 177092.4) and glyceraldehyde-3-phosphate dehydrogenase (*Gapdh*) (NM001289726.1). For RT-PCR, we used primers that specifically amplified a portion of exon 7 of the *MsrB3* gene because exon 7 was eliminated in the *MsrB3*$^{-/-}$ mice. This PCR allowed us to compare samples from the *MsrB3*$^{+/+}$ mice with those from the untreated right ears and treated left ears of the rescued *MsrB3*$^{-/-}$ mice. The *Gapdh* gene was used as a positive control and was amplified in all samples. The following PCR primer sequences were used: *MsrB3* forward, CTC CCC TCA GGG TCA TGT AGG; *MsrB3* reverse, AGC ACC ACA CTG AGA ACA GC; *Gapdh* forward, GGT GCT GAG TAT GTC GTG GA; and *Gapdh* reverse, CTA AGC AGT TGG TGG TGC AG. All of the PCR products were separated *via* agarose gel electrophoresis (1.5% agarose gels containing ethidium bromide) and then visualized under ultraviolet (UV) light.

Western blot analysis

Each inner ear was homogenized in lysis buffer containing a 1× protease inhibitor cocktail (Calbiochem, La Jolla, CA) for 30 min at 4°C and then centrifuged at 13,000 rpm for 30 min. Then, the content of the supernatant was resolved *via* 12% sodium dodecyl sulfate–polyacrylamide gel electrophoresis. The proteins were detected using a rabbit anti-MsrB3 primary antibody (1:500; Sigma-Aldrich) and a goat anti-rabbit IgG-HRP (1:2000; Santa Cruz Biotechnology, Santa Cruz, CA) secondary antibody. A rabbit anti-β-actin antibody (1:2000; Cell Signaling Technology, Beverly, MA) and a goat anti-rabbit IgG-HRP antibody (1:2000; Santa Cruz Biotechnology) were used to detect β-actin, which was used as a loading control. Protein expression was visualized using an enhanced chemiluminescence system (Thermo Fisher Scientific, Pittsburgh, PA). The intensity of each MsrB3 and

β-actin band was measured using ImageJ software (http://rsb.info.nih.gov/ij/), and MsrB3 signals were quantified by normalization to the expression of β-actin.

Paraffin sections

Following ABR testing, the mice were perfused with 4% PFA in PBS, and the inner ears were isolated. For paraffin sections, the inner ears were fixed with 4% PFA in PBS for 24 h at 4°C and then decalcified in 10% ethylenediaminetetraacetic acid (EDTA) in PBS for another 24 h at 4°C. The specimens were dehydrated with a graded ethanol series, permeabilized with xylene, and embedded in paraffin at RT. The paraffin-embedded inner ears were then serially sectioned into 5-μm-thick slices using a microtome (Leica RM2235; Leica Microsystems, Wetzlar, Germany) and mounted on Superfrost Plus microscope slides (Thermo Fisher Scientific) for staining. All slides were maintained at 4°C until use.

Immunohistochemistry

The expression of rAAV2/1-*MsrB3-GFP* in the inner ear was determined *via* immunofluorescence in paraffin sections. The slides of paraffin-embedded inner ear sections were incubated for 1 h at 65°C, deparaffinized with xylene, and rehydrated with a graded ethanol series. The tissue sections were permeabilized with PBS-Tx for 30 min, blocked using a blocking solution comprising 5% normal goat serum and PBS-Tx for 1 h at RT, and incubated at 4°C overnight with a mouse anti-GFP antibody (1:400; Millipore Filter Corporation), a mouse anti-Myo7a antibody (1:500; Developmental Studies Hybridoma Bank, Iowa City, IA), or a rabbit anti-MsrB3 antibody (1:200; Sigma-Aldrich) diluted in the blocking solution. The next day, the tissue sections were washed with PBS and then incubated for 1 h at RT with the appropriate secondary antibody, which was either an Alexa Fluor 488 (fluorescein)-conjugated goat anti-mouse IgG antibody (1:1000; Invitrogen) or an Alexa Fluor 555-conjugated goat anti-rabbit IgG antibody (1:1000; Invitrogen) diluted in the blocking solution. To visualize nuclei, the sections were washed and stained with a 1 μg/ml 4′-6-diamidino-2-phenylindole (DAPI) solution diluted in methanol for 5 min at RT. The samples were washed with PBS to remove any residual antibodies, mounted with Fluoromount (Sigma-Aldrich), and sealed with a microscope coverslip (Marienfeld Laboratory). All slides were observed under a laser scanning confocal microscope (LSM 700; Carl Zeiss).

Scanning electron microscopy

The inner ears were immediately harvested from the euthanized WT, *MsrB3*$^{-/-}$, and rescued *MsrB3*$^{-/-}$ mice and carefully perfused through the oval window with a solution of 2% PFA dissolved in 0.1 *M* sodium cacodylate buffer (pH 7.4) containing 2.5% glutaraldehyde. The prepared specimens were immersed in the same fixative for 1 h at RT. The lateral wall, tectorial membrane, and Reissner's membrane were removed under a dissecting microscope, and the organ of Corti was then dissected and fixed overnight at 4°C in a fixation mixture comprising 0.1 *M* sodium cacodylate buffer (pH 7.4), 2 m*M* calcium chloride, 2.5% glutaraldehyde, and 3.5% sucrose. Following fixation, the prepared specimens were washed thrice for 20 min at 4°C with 0.1 *M* sodium cacodylate buffer containing 2 m*M* calcium chloride. We used the method of Hunter-Duvar (17) for postfixation analysis. Briefly, the specimens were immersed in a 1% osmium tetroxide (OsO_4)–thiocarbohydrazide (TCH) solution for 1 h at 4°C and placed in 1% TCH for 20 min at RT. These steps were repeated thrice. Then, the specimens were dehydrated in a graded ethanol series, dried using a critical point dryer (HCP-2; Hitachi, Tokyo, Japan), attached on the stub, and coated with platinum using a sputter coater (E1030; Hitachi). The coated specimens were sealed with the stub holder. The specimens were examined under cold-field emission SEM (SU8220; Hitachi) that was operated at 5 or 10 kV.

Statistical analyses

Statistical analyses were performed using two-tailed Student's *t*-tests with a significance criterion of $p < 0.05$. The data were analyzed by comparing the treated and the untreated contralateral sides or the therapy and control groups.

Study approval

All animal procedures, including care and handling, were conducted in accordance with the guidelines of the Institutional Animal Care issued by the Committee of Animal Research at Kyungpook National University.

Acknowledgments

The authors especially thank Dr. Dennis Drayna and Dr. Doris Wu for comments on the manuscript. The research was supported by a grant from the Korea Health Technology R&D Project through the Korea Health Industry Development Institute (KHIDI), funded by the Ministry of Health and Welfare, Republic of Korea (Grant Number: HI14C2119).

Author Contributions

M.-A.K. performed the experiments, analyzed the data, and wrote the manuscript; H.-J.C. performed the experiments and wrote the manuscript; S.-H.B., B.L., S.-K.O., and T.-J.K. performed the experiments; Z.-Y.R., H.-Y.K., and J.-H.C. provided important reagents and mice; and K.-Y.L. and U.-K.K. designed the study, analyzed the data, and wrote the manuscript.

Author Disclosure Statement

No competing financial interests exist.

References

1. Ahmed ZM, Yousaf R, Lee BC, Khan SN, Lee S, Lee K, Husnain T, Rehman AU, Bonneux S, Ansar M, Ahmad W, Leal SM, Gladyshev VN, Belyantseva IA, Van Camp G, Riazuddin S, Friedman TB, and Riazuddin S. Functional null mutations of MSRB3 encoding methionine sulfoxide reductase are associated with human deafness DFNB74. *Am J Hum Genet* 88: 19–29, 2011.
2. Akil O, Seal RP, Burke K, Wang C, Alemi A, During M, Edwards RH, and Lustig LR. Restoration of hearing in the VGLUT3 knockout mouse using virally mediated gene therapy. *Neuron* 75: 283–293, 2012.
3. Atkinson PJ, Wise AK, Flynn BO, Nayagam BA, and Richardson RT. Hair cell regeneration after ATOH1 gene therapy in the cochlea of profoundly deaf adult guinea pigs. *PLoS One* 9: e102077, 2014.

4. Bedrosian JC, Gratton MA, Brigande JV, Tang W, Landau J, and Bennett J. In vivo delivery of recombinant viruses to the fetal murine cochlea: transduction characteristics and long-term effects on auditory function. *Mol Ther* 14: 328–335, 2006.
5. Berlett BS and Stadtman ER. Protein oxidation in aging, disease, and oxidative stress. *J Biol Chem* 272: 20313–20316, 1997.
6. Cao G, Lee KP, van der Wijst J, de Graaf M, van der Kemp A, Bindels RJ, and Hoenderop JG. Methionine sulfoxide reductase B1 (MsrB1) recovers TRPM6 channel activity during oxidative stress. *J Biol Chem* 285: 26081–26087, 2010.
7. Ciorba MA, Heinemann SH, Weissbach H, Brot N, and Hoshi T. Modulation of potassium channel function by methionine oxidation and reduction. *Proc Natl Acad Sci U S A* 94: 9932–9937, 1997.
8. Gabbita SP, Aksenov MY, Lovell MA, and Markesbery WR. Decrease in peptide methionine sulfoxide reductase in Alzheimer's disease brain. *J Neurochem* 73: 1660–1666, 1999.
9. Gillespie LN, Richardson RT, Nayagam BA, and Wise AK. Treating hearing disorders with cell and gene therapy. *J Neural Eng* 11: 065001, 2014.
10. Groves AK. The challenge of hair cell regeneration. *Exp Biol Med (Maywood)* 235: 434–446, 2010.
11. Heffer LF, Sly DJ, Fallon JB, White MW, Shepherd RK, and O'Leary SJ. Examining the auditory nerve fiber response to high rate cochlear implant stimulation: chronic sensorineural hearing loss and facilitation. *J Neurophysiol* 104: 3124–3135, 2010.
12. Henderson LB, Doshi VK, Blackman SM, Naughton KM, Pace RG, Moskovitz J, Knowles MR, Durie PR, Drumm ML, and Cutting GR. Variation in MSRA modifies risk of neonatal intestinal obstruction in cystic fibrosis. *PLoS Genet* 8: e1002580, 2012.
13. Hildebrand MS, Newton SS, Gubbels SP, Sheffield AM, Kochhar A, de Silva MG, Dahl HH, Rose SD, Behlke MA, and Smith RJ. Advances in molecular and cellular therapies for hearing loss. *Mol Ther* 16: 224–236, 2007.
14. Hoshi T and Heinemann S. Regulation of cell function by methionine oxidation and reduction. *J Physiol* 531: 1–11, 2001.
15. Hung RJ, Pak CW, and Terman JR. Direct redox regulation of F-actin assembly and disassembly by Mical. *Science* 334: 1710–1713, 2011.
16. Hung RJ, Yazdani U, Yoon J, Wu H, Yang T, Gupta N, Huang Z, van Berkel WJ, and Terman JR. Mical links semaphorins to F-actin disassembly. *Nature* 463: 823–827, 2010.
17. Hunter-Duvar IM. A technique for preparation of cochlear specimens for assessment with the scanning electron microscope. *Acta Otolaryngol Suppl* 351: 3–23, 1978.
18. Imlay JA. Cellular defenses against superoxide and hydrogen peroxide. *Annu Rev Biochem* 77: 755–776, 2008.
19. Jecmenica J, Bajec-Opancina A, and Jecmenica D. Genetic hearing impairment. *Childs Nerv Syst* 31: 515–519, 2015.
20. Jero J, Mhatre AN, Tseng CJ, Stern RE, Coling DE, Goldstein JA, Hong K, Zheng WW, Hoque AT, and Lalwani AK. Cochlear gene delivery through an intact round window membrane in mouse. *Hum Gene Ther* 12: 539–548, 2001.
21. Konishi M, Kawamoto K, Izumikawa M, Kuriyama H, and Yamashita T. Gene transfer into guinea pig cochlea using adeno-associated virus vectors. *J Gene Med* 10: 610–618, 2008.
22. Krause KH. Aging: a revisited theory based on free radicals generated by NOX family NADPH oxidases. *Exp Gerontol* 42: 256–262, 2007.
23. Kryukov GV, Kumar RA, Koc A, Sun Z, and Gladyshev VN. Selenoprotein R is a zinc-containing stereo-specific methionine sulfoxide reductase. *Proc Natl Acad Sci U S A* 99: 4245–4250, 2002.
24. Kwon TJ, Cho HJ, Kim UK, Lee E, Oh SK, Bok J, Bae YC, Yi JK, Lee JW, Ryoo ZY, Lee SH, Lee KY, and Kim HY. Methionine sulfoxide reductase B3 deficiency causes hearing loss due to stereocilia degeneration and apoptotic cell death in cochlear hair cells. *Hum Mol Genet* 23: 1591–1601, 2014.
25. This reference has been deleted.
26. Lee BC, Dikiy A, Kim HY, and Gladyshev VN. Functions and evolution of selenoprotein methionine sulfoxide reductases. *Biochim Biophys Acta* 1790: 1471–1477, 2009.
27. Lee BC, Peterfi Z, Hoffmann FW, Moore RE, Kaya A, Avanesov A, Tarrago L, Zhou Y, Weerapana E, Fomenko DE, Hoffmann PR, and Gladyshev VN. MsrB1 and MICALs regulate actin assembly and macrophage function via reversible stereoselective methionine oxidation. *Mol Cell* 51: 397–404, 2013.
28. Lee HJ, Jung J, Shin JW, Song MH, Kim SH, Lee JH, Lee KA, Shin S, Kim UK, Bok J, Lee KY, Choi JY, and Park HJ. Correlation between genotype and phenotype in patients with bi-allelic SLC26A4 mutations. *Clin Genet* 86: 270–275, 2014.
29. Lee HJ, Yoo SJ, Lee S, Song HJ, Huh MI, Jin SU, Lee KY, Lee J, Cho JH, and Chang Y. Functional activity mapping of rat auditory pathway after intratympanic manganese administration. *Neuroimage* 60: 1046–1054, 2012.
30. Minoda R, Miwa T, Ise M, and Takeda H. Potential treatments for genetic hearing loss in humans: current conundrums. *Gene Ther* 22: 603–609, 2015.
31. Miwa T, Minoda R, Ise M, Yamada T, and Yumoto E. Mouse otocyst transuterine gene transfer restores hearing in mice with connexin 30 deletion-associated hearing loss. *Mol Ther* 21: 1142–1150, 2013.
32. Moskovitz J. Methionine sulfoxide reductases: ubiquitous enzymes involved in antioxidant defense, protein regulation, and prevention of aging-associated diseases. *Biochim Biophys Acta* 1703: 213–219, 2005.
33. Moskovitz J, Berlett BS, Poston JM, and Stadtman ER. The yeast peptide-methionine sulfoxide reductase functions as an antioxidant in vivo. *Proc Natl Acad Sci U S A* 94: 9585–9589, 1997.
34. Moskovitz J, Rahman MA, Strassman J, Yancey SO, Kushner SR, Brot N, and Weissbach H. *Escherichia coli* peptide methionine sulfoxide reductase gene: regulation of expression and role in protecting against oxidative damage. *J Bacteriol* 177: 502–507, 1995.
35. Oien DB, Ortiz AN, Rittel AG, Dobrowsky RT, Johnson MA, Levant B, Fowler SC, and Moskovitz J. Dopamine D(2) receptor function is compromised in the brain of the methionine sulfoxide reductase A knockout mouse. *J Neurochem* 114: 51–61, 2010.
36. Oien DB, Osterhaus GL, Latif SA, Pinkston JW, Fulks J, Johnson M, Fowler SC, and Moskovitz J. MsrA knockout mouse exhibits abnormal behavior and brain dopamine levels. *Free Radic Biol Med* 45: 193–200, 2008.
37. Pal R, Oien DB, Ersen FY, and Moskovitz J. Elevated levels of brain-pathologies associated with neurodegenerative diseases in the methionine sulfoxide reductase A knockout mouse. *Exp Brain Res* 180: 765–774, 2007.
38. Pang JJ, Boye SL, Kumar A, Dinculescu A, Deng W, Li J, Li Q, Rani A, Foster TC, Chang B, Hawes NL, Boatright JH, and Hauswirth WW. AAV-mediated gene therapy for retinal degeneration in the rd10 mouse containing a

recessive PDEbeta mutation. *Invest Ophthalmol Vis Sci* 49: 4278–4283, 2008.
39. Patuzzi RB, Yates GK, and Johnstone BM. Outer hair cell receptor current and sensorineural hearing loss. *Hear Res* 42: 47–72, 1989.
40. Rivolta MN. New strategies for the restoration of hearing loss: challenges and opportunities. *Br Med Bull* 105: 69–84, 2012.
41. Rodrigo MJ, Moskovitz J, Salamini F, and Bartels D. Reverse genetic approaches in plants and yeast suggest a role for novel, evolutionarily conserved, selenoprotein-related genes in oxidative stress defense. *Mol Genet Genomics* 267: 613–621, 2002.
42. Santarelli LC, Wassef R, Heinemann SH, and Hoshi T. Three methionine residues located within the regulator of conductance for K+ (RCK) domains confer oxidative sensitivity to large-conductance Ca2+-activated K+ channels. *J Physiol* 571: 329–348, 2006.
43. Shepherd RK and Hardie NA. Deafness-induced changes in the auditory pathway: implications for cochlear implants. *Audiol Neurootol* 6: 305–318, 2001.
44. Singh VK and Moskovitz J. Multiple methionine sulfoxide reductase genes in *Staphylococcus aureus*: expression of activity and roles in tolerance of oxidative stress. *Microbiology* 149: 2739–2747, 2003.
45. Sinha K, Das J, Pal PB, and Sil PC. Oxidative stress: the mitochondria-dependent and mitochondria-independent pathways of apoptosis. *Arch Toxicol* 87: 1157–1180, 2013.
46. Skaar EP, Tobiason DM, Quick J, Judd RC, Weissbach H, Etienne F, Brot N, and Seifert HS. The outer membrane localization of the *Neisseria gonorrhoeae* MsrA/B is involved in survival against reactive oxygen species. *Proc Natl Acad Sci U S A* 99: 10108–10113, 2002.
47. Stadtman ER. Protein oxidation and aging. *Free Radic Res* 40: 1250–1258, 2006.
48. Stadtman ER and Levine RL. Free radical-mediated oxidation of free amino acids and amino acid residues in proteins. *Amino Acids* 25: 207–218, 2003.
49. Stadtman ER, Moskovitz J, Berlett BS, and Levine RL. Cyclic oxidation and reduction of protein methionine residues is an important antioxidant mechanism. *Mol Cell Biochem* 234–235: 3–9, 2002.
50. Stadtman ER, Moskovitz J, and Levine RL. Oxidation of methionine residues of proteins: biological consequences. *Antioxid Redox Signal* 5: 577–582, 2003.
51. Stone IM, Lurie DI, Kelley MW, and Poulsen DJ. Adeno-associated virus-mediated gene transfer to hair cells and support cells of the murine cochlea. *Mol Ther* 11: 843–848, 2005.
52. Stone JS, Oesterle EC, and Rubel EW. Recent insights into regeneration of auditory and vestibular hair cells. *Curr Opin Neurol* 11: 17–24, 1998.
53. Ugarte N, Petropoulos I, and Friguet B. Oxidized mitochondrial protein degradation and repair in aging and oxidative stress. *Antioxid Redox Signal* 13: 539–549, 2010.
54. Wilson C and Gonzalez-Billault C. Regulation of cytoskeletal dynamics by redox signaling and oxidative stress: implications for neuronal development and trafficking. *Front Cell Neurosci* 9: 381, 2015.
55. Yagi M, Kanzaki S, Kawamoto K, Shin B, Shah PP, Magal E, Sheng J, and Raphael Y. Spiral ganglion neurons are protected from degeneration by GDNF gene therapy. *J Assoc Res Otolaryngol* 1: 315–325, 2000.

Address correspondence to:
Prof. Kyu-Yup Lee
Department of Otorhinolaryngology-Head and Neck Surgery
School of Medicine
Kyungpook National University
Daegu 41944
Republic of Korea

E-mail: kylee@knu.ac.kr

Prof. Un-Kyung Kim
Department of Biology
College of Natural Sciences
Kyungpook National University
Daegu 41566
Republic of Korea

E-mail: kimuk@knu.ac.kr

Date of first submission to ARS Central, July 10, 2015; date of final revised submission, November 18, 2015; date of acceptance, December 7, 2015.

Abbreviations Used

ABR = auditory brainstem response
CAG = CMV early enhancer/chicken β-actin
cDNA = complementary DNA
CI = cochlear implantation
CMV = cytomegalovirus
Cx30 = connexin 30
DAPI = 4′-6-diamidino-2-phenylindole
E = embryonic day
EDTA = ethylenediaminetetraacetic acid
Gapdh = glyceraldehyde-3-phosphate dehydrogenase
GFP = green fluorescent protein
ICR = Institute for Cancer Research
IHC = inner hair cell
i.m. = intramuscular
ITR = inverted terminal repeat
MsrA = methionine sulfoxide reductase A
MsrB3 = methionine sulfoxide reductase B3
OHC = outer hair cell
OsO_4 = osmium tetroxide
P = postnatal day
PBS = phosphate-buffered saline
PBS-Tx = triton X-100 in PBS
PCR = polymerase chain reaction
PFA = paraformaldehyde
rAAV = recombinant adeno-associated virus
ROS = reactive oxygen species
RT = room temperature
RT-PCR = reverse transcription–polymerase chain reaction
SEM = scanning electron microscopy
SNHL = sensorineural hearing loss
TCH = thiocarbohydrazide
TDT = Tucker Davis Technology
Vglut3 = vesicular glutamate transporter 3
WT = wild-type